In situ Polarized Neutron Reflectometry: Epitaxial Thin-Film Growth of Fe on Cu(001) by dc Magnetron Sputtering

Wolfgang Kreuzpaintner,[1,*] Birgit Wiedemann,[1] Jochen Stahn,[2] Jean-François Moulin,[3] Sina Mayr,[1] Thomas Mairoser,[4] Andreas Schmehl,[4] Alexander Herrnberger,[4] Panagiotis Korelis,[2] Martin Haese,[3] Jingfan Ye,[1] Matthias Pomm,[3] Peter Böni,[1] and Jochen Mannhart[5]

[1]*Technische Universität München, Physik-Department E21, James-Franck-Straße 1, 85748 Garching, Germany*

[2]*Laboratory for Neutron Scattering and Imaging, Paul Scherrer Institut, 5232 Villigen PSI, Switzerland*

[3]*Helmholtz-Zentrum Geesthacht, Zentrum für Material und Küstenforschung, Außenstelle am MLZ in Garching bei München, Lichtenbergstraße 1, 85748 Garching, Germany*

[4]*Zentrum für elektronische Korrelation und Magnetismus, Universität Augsburg, Lehrstuhl für Experimentalphysik VI, Universitätsstraße 1, 86159 Augsburg, Germany*

[5]*Max-Planck-Institut für Festkörperforschung, Heisenbergstraße 1, 70569 Stuttgart, Germany*

(Received 11 October 2016; revised manuscript received 26 February 2017; published 9 May 2017)

The stepwise growth of epitaxial Fe on Cu(001)/Si(001), investigated by *in situ* polarized neutron reflectometry is presented. A sputter deposition system was integrated into the neutron reflectometer AMOR at the Swiss neutron spallation source SINQ, which enables the analysis of the microstructure and magnetic moments during all deposition steps of the Fe layer. We report on the progressive evolution of the accessible parameters describing the microstructure and the magnetic properties of the Fe film, which reproduce known features and extend our knowledge on the behavior of ultrathin iron films.

DOI: 10.1103/PhysRevApplied.7.054004

I. INTRODUCTION

Owing to their valuable electronic, magnetic, and optical properties, thin films and heterostructures are indispensable in scientific and technological applications and offer fascinating prospects for the realization of advanced electronic devices [1–11]. As a result, an increasing number of thin films and heterostructures are grown with atomic-layer precision by means of physical vapor deposition from complex materials [12]. The material spectrum also broadens; sophisticated heterostructures of high complexity use a steadily increasing number of elements of the periodic table [13,14]. At the same time, the control of defects and intended sample properties becomes more relevant. As morphologies, including sample structure, stoichiometry, and defect population evolve with the deposition, so do the magnetic properties of the sample. It is, hence, highly desirable—and even more challenging—to analyze both as a function of layer thickness *in situ*. While the *in situ* characterization of films by electron- and photon-based probes [15,16] as well as by scanning probe techniques [17,18] is common practice, only a few attempts have been made to characterize the emerging sample properties by neutron scattering [19–21]. However, as a spin-sensitive technique, polarized neutron reflectometry (PNR) is very sensitive to both structural and magnetic properties with atomic resolution. It is, hence, well established as an indispensable *ex situ* method to investigate samples in their final state. If it were possible to routinely perform PNR *in situ* on growing films and heterostructures, PNR would be even more valuable, as it can contribute to answering the grand questions of how the microstructure, defects, and, if applicable, magnetic properties of heterostructures (i) form, (ii) are correlated with each other, and (iii) evolve during growth. The results will be particularly valuable because all PNR data are accumulated from the very same sample.

As neutron sources and neutron optical concepts have strongly evolved in the last decades, and with data storage densities approaching regimes where a fundamental understanding of magnetism on the atomic scale is the key for further progress, today *in situ* PNR appears as a forthcoming analytical technique.

Therefore, we decided to investigate the current state of viability and the potential of *in situ* PNR in the context of analyzing the progressive evolution of the accessible microstructure parameters and the magnetic properties of a sputter-deposited epitaxial Fe film on a $Cu(001)_{45\ nm}/Si(001)$ substrate. This sample type is specifically chosen, as its structural and accompanying magnetic properties have been widely studied in the past for different deposition and analysis techniques on a variety of substrates [22–28], yet, only little work has been done on sputter-deposited Fe thin films [29]. Any potentially different growth mode and a deviating magnetic behavior of sputtered films could provide both more insight into the physics of thin magnetic films and a benchmarking of the *in situ* PNR method.

As today's neutron sources do not yet provide the required brilliance for *in operando* PNR experiments,

*wolfgang.kreuzpaintner@frm2.tum.de

the data presented in the following are taken while the coating process is periodically interrupted for the *in situ* PNR measurements. In order to avoid potential surface contamination, special attention is given to a compatibility of the vacuum quality of our *in situ* thin-film deposition setup with the required neutron-data acquisition times. The coating setup offers a base pressure of 5.0×10^{-9} mbar, which is created by a turbomolecular pump (TMP). Because of the TMP's working principle of momentum transfer, the main constituent of the residual gas in the vacuum chamber is H_2, which only weakly interacts with the Fe surface. Contaminating residual gas species are typically 2 orders of magnitude below H_2, such that a monolayer formation time of $\sim 10^4$–10^5 s can be assumed. To further rule out any contaminating influences from residual gas species, we aim at reducing our *in situ* PNR data acquisition times to the lowest possible value by combining our *in situ* deposition setup with the prototype of the focusing Selene neutron optical concept [30,31]. It uses a pair of Montel mirrors to focus a broad-wavelength-band neutron beam onto the sample and is capable of providing the data within 15 min per spin direction for our *in situ* PNR measurements. The data acquisition times are therefore sufficiently fast to avoid any relevant contamination of the Fe surface before the next Fe deposition step is performed.

II. EXPERIMENTAL PROCEDURE

A. *In situ* thin-film preparation

The coating setup is equipped with three 2-inch sputter-deposition sources, which are operated in direct current (dc) mode. The sputter guns are implemented such that either of the sputter sources can be rotated to a position perpendicular to the sample surface. A schematic cross section and details of the sputtering system are shown in Fig. 1. In-vacuum guide fields are implemented to maintain the neutron polarization up to the sample position. Stepping motors on linear and rotary vacuum feedthroughs are used to align the sample in the neutron beam. A more detailed design description of the deposition setup will be presented elsewhere. The thin films are deposited epitaxially *in situ* in the neutron beam using metal-metal epitaxy on silicon [32–37]. After a 45-nm-thick Cu(001) seed layer, a 7.0-nm-thick Fe layer is grown in 28 separate deposition steps i from a 99.99% pure Fe sputter target at an Ar sputtering gas [38] pressure of 4.50×10^{-3} mbar. The dc sputtering power of 20 W results in a deposition rate of 0.18 $\mu g\,cm^{-2}\,s^{-1}$. The deposition of the equivalent of approximately 1 monolayer of Fe per deposition step is controlled by the opening times of a deposition shutter (typically 1.5 s per deposition step). Between two deposition steps the chamber is evacuated to base pressure and the *in situ* PNR measurements are carried out. After the 14th Fe deposition step, the *in situ* PNR measurements are performed only after every second coating step.

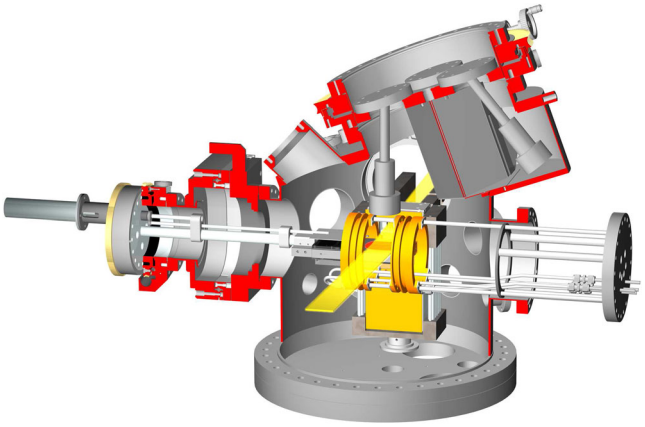

FIG. 1. Schematic cross section of the *in situ* sputter-deposition chamber: the sample manipulator is mounted on the left flange. The sample, exposed to the neutron beam (sketched in yellow) is located in the center. A retractable pair of Helmholtz coils, used to magnetize the sample, is mounted at the right flange. For magnetic fields exceeding 30 mT, the coils are replaced by permanent magnets. The three sputter sources are located on the top, separated by shields to avoid cross contamination.

B. *In situ* polarized neutron reflectometry

The unique feature of the AMOR beam line at the Paul Scherrer Institut is that most components are mounted on an optical bench. The instrument is, therefore, highly flexible and allows both the installation of the *in situ* sputter-deposition chamber and the insertion of the prototype of the Selene neutron guide [30,31]. It ends 400 mm before the focal point and is fully compatible with the deposition setup, where the distance from the fused silica (SiO_2) neutron window of the *in situ* deposition setup to the sample is 380 mm.

Figure 2 shows the integration of the coating setup and the Selene optics into AMOR. The sputter process is controlled remotely. For the *in situ* PNR measurements a magnetic field of 70 mT is applied to the sample perpendicular to the scattering plane using permanent magnets. Since in the Selene mode the complete beam is convergent and the sample is in the focal point, no further beam-shaping elements between the optics and the sample are needed and the full beam divergence of 1.6° is used to illuminate the sample with a neutron wavelength band of 4–10 Å. This leads to a gain factor of 30 when compared to the conventional PNR operation mode of AMOR. However, the resolution in $\Delta q_z/q_z$ becomes q_z dependent (see Ref. [31] for details). With the settings applied for our measurements, the resolution quickly increases from $\Delta q_z/q_z \approx 4.5\%$ in the regime of total reflection to a quasistable value of $\Delta q_z/q_z \approx 2.3\%$ for $q_z \gtrsim 0.2$ nm^{-1}. Beam polarization is realized by the transmittance of the neutrons through an $m = 4.2$ Fe/Si multilayer polarizer with a logarithmic spiral shape. The neutron polarization is selected by an rf spin flipper.

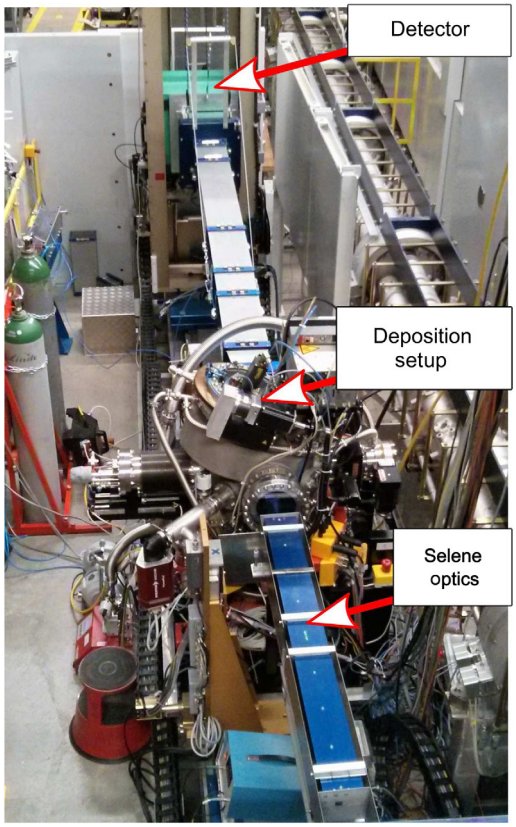

FIG. 2. Sputter-deposition chamber and Selene optics, integrated into the AMOR beam line: The *in situ* chamber is located in the center of the beam. Clearly visible is the neutron window made from fused silica (SiO_2). The neutrons leave the vacuum chamber on the opposite side through an identical window, followed by a flight tube made from aluminum and the two-dimensional detector (turquoise box). The blue Selene guide elements are located in front of the sputtering chamber.

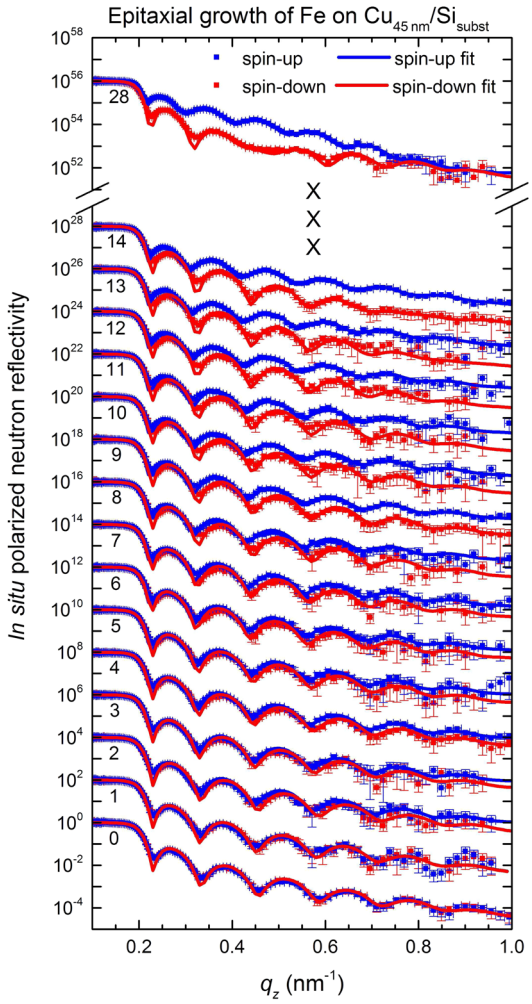

FIG. 3. Measured *in situ* PNR data, overlaid with fitted reflectivity curves. Shown is the neutron reflectivity versus the perpendicular momentum transfer q_z. Each pair of curves is vertically shifted by 2 orders of magnitude for better visibility. Typically, the *in situ* PNR data acquisition time is 15 min per spin direction. The number below the regime of total reflection denotes the deposition step i of the epitaxial Fe layer. Each deposition step between the *in situ* PNR measurements requires approximately 5 min.

III. RESULTS AND DISCUSSION

The *in situ* PNR data overlaid with the fitted reflectivity curves is shown in Fig. 3. Each pair is characterized by four key parameters: (a) the critical edge up to which total reflection occurs, revealing the scattering length density from which the number density of each layer (n^{Cu} and n^{Fe}) is obtained; (b) the periodic Kiessig fringes, a measure of the layer thickness d^{Cu} and d^{Fe}; (c) the decay of the reflectivity curves that exceeds the expected decrease in the Fresnel reflectivity, a measure for the interfacial root-mean-square (rms) roughness $\sigma^{\mathrm{Cu/Si}}$ on the Cu/Si and $\sigma^{\mathrm{Fe/Cu}}$ on the Fe/Cu interfaces; and (d) the splitting of the spin-up (+) and spin-down (−) reflectivity R^+ and R^-, providing quantitative information on the magnetic moments in the sample.

While for the deposition step $i = 1$ R^+ and R^- are identical, the gradual increase in the splitting between R^+ and R^- from $i = 2$ to $i = 28$ directly correlates with the magnitude of the in-plane magnetization M^{Fe} of the Fe layer and with d^{Fe}. The *in situ* PNR data are analyzed quantitatively using the SimulReflec Software Package [39] assuming a two-layer model: Fe on $\mathrm{Cu}_{\mathrm{seed}}$ on Si substrate. The parameters of the Cu layer, i.e., $d^{\mathrm{Cu}} = 45.14\binom{+0.21}{-0.14}$ nm, $n^{\mathrm{Cu}} = 8.36\binom{+0.19}{-0.11} \times 10^{22}$ cm^{-3}, and $\sigma^{\mathrm{Cu/Fe}} = 0.63\binom{+0.12}{-0.18}$ nm are kept constant while the parameters of the Fe layer are varied.

The resulting fit parameters d_i^{Fe}, n_i^{Fe} (10^{22} cm^{-3}), σ_i^{Fe}, and M_i^{Fe} (μ_{Bohr}/atom) and their evolution are shown in Fig. 4 as a function of i and the amount of deposited material. The errors of the Cu and Fe parameters are estimated by a 5% increase over the optimum figure of merit $\mathrm{FOM} \sim \sum |\ln R_{\mathrm{fit}} - \ln R_{\mathrm{meas}}|$ on an independent

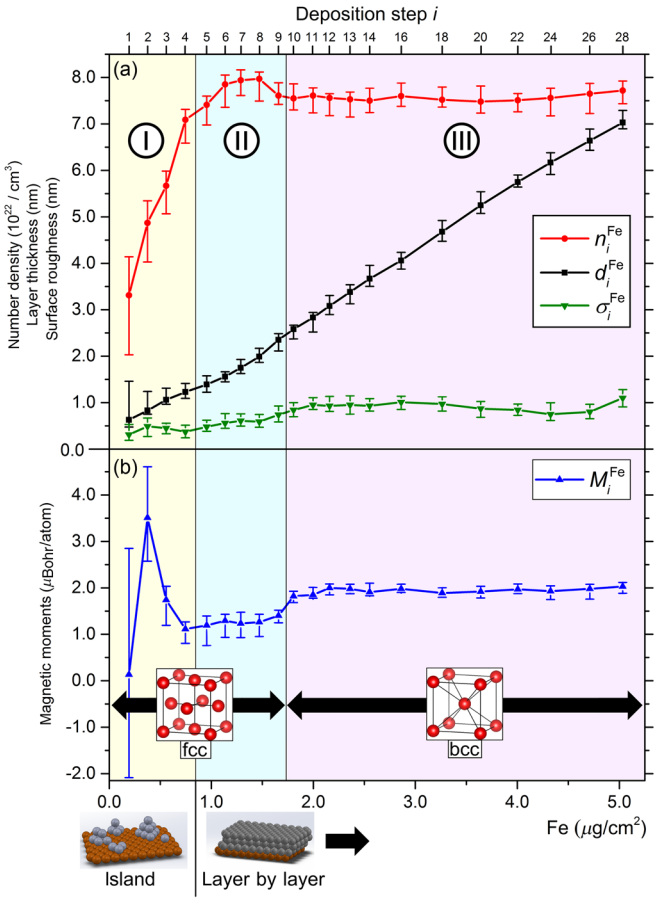

FIG. 4. The fit parameters of the epitaxially grown Fe layer. Three main regimes (I–III) with different characteristic behaviors for the number density n_i^{Fe}, thickness d_i^{Fe}, interfacial roughness σ_i^{Fe}, and magnetization M_i^{Fe} can be identified. Shown are also the concluded growth modes (island and layer by layer) and crystalline structures (fcc and bcc).

variation of a single parameter [40], where R_{fit} is the fitted and R_{meas} the measured reflectivity, respectively.

Three regimes I–III in the evolution of the fit parameters can be identified.

Regime I.—The deposition step $i = 1$ generates an Fe layer with an apparent thickness of $d_1^{Fe} = 0.63$ nm (approximately three monolayers) and a very low number density of Fe atoms: $n_1^{Fe} = 3.31 \times 10^{22}/\text{cm}^3$ if compared to the bulk value ($\sim 8.48 \times 10^{22}/\text{cm}^3$). This density can only be rationalized by requiring the scattering length density of the layer to be composed of a weighted average of the scattering lengths of Fe ($b^{Fe} = 3.31$ fm) and vacuum ($b^{vac} = 0$ fm). The low density implies that either the first three monolayers form islands or a layer of very small density.

The data of the following deposition steps $2 \leq i < 5$ indicate, too, that the film indeed starts its growth in the island mode [41,42], because these steps yield only a small relative increase in thickness but a density n_i^{Fe}, which increases significantly faster than d_i^{Fe}. The simultaneously occurring reduction of surface roughness for steps $3 \leq i \leq 5$ relative to the thickness of the layers also traces the coalescence of separate Fe islands. Interestingly, the coating applied in deposition step $i = 1$ shows an in-plane magnetization of a mere $0.13\mu_{Bohr}$/atom, which we attribute to a strong perpendicular magnetic anisotropy [42–46] or superparamagnetism of nanoscale islands [47,48].

While the density and the thickness of the layers increase continuously with each deposition step, the in-plane magnetization varies strongly. After $i = 2$ ($d_2^{Fe} = 0.83$ nm) the film exhibits an in-plane magnetization of $3.5\mu_{Bohr}$/atom. Ultrathin Fe layers on various substrates with a magnetization exceeding the bulk level have been reported before [45,49–51] and are confirmed by our measurements, yet the magnetization in our film in its nucleation phase might exceed even these large literature values of up to $\sim 3.1\mu_{Bohr}$/atom [50,51]. At the deposition step $i = 4$, the magnetization has decreased from its maximum ($i = 2$) to a level of $\sim 1.25\mu_{Bohr}$/atom, where it remains approximately constant up to growth step $i = 9$.

Regime II.—After the deposition step $i = 4$, the Fe islands have completely coalesced, as revealed by the change in the increase in thickness from 0.95 nm/(μg cm^{-2}) for $3 \leq i \leq 4$ to 1.35 nm/(μg cm^{-2}) for $i > 4$, which coincides with the phasing out of the increase in density ($4 \leq i \leq 5$). A transition to a layer-by-layer growth with the 5th deposition step must, therefore, be concluded. The density of the Fe layer reaches a value of $\sim 7.95 \times 10^{22}/\text{cm}^3$ ($6 \leq i \leq 8$).

The evolvement of the magnetism is directly visible in *in situ* PNR by the clear separation of the spin-polarized raw data. Room-temperature magnetism of Fe thin films has previously only been reported for thicknesses below ~4 [43–46] and above 12 atomic layers [46]. According to the literature, Fe films with a thickness of 5–11 atomic layers have a Curie temperature T_C of only 275–280 K [46]. The increase in T_C to above room temperature in our experiment falls in line with the enhanced magnetization of the film shown during its nucleation. We attribute the enhancement of the magnetization to the microstructure of the *in situ* grown films differing from the ones of the Fe films reported in the literature [46] caused by the use of sputtering as the deposition method.

An oscillatory magnetic behavior [43,44,52], resulting from antiferromagnetic coupling between single atomic Fe layers with intrinsic perpendicular magnetization could not be confirmed in our *in situ* PNR measurements. It is noted that the applied magnetic field of 70 mT may have been sufficiently strong to overcome the anisotropy, rotating the magnetic moments in plane and thereby suppressing these oscillations [42,53].

Regime III.—As the film continues to grow through steps $8 \leq i \leq 12$, its number density decreases to $\sim 7.6 \times 10^{22}/\text{cm}^3$. In parallel, the interfacial roughness increases slightly, and the magnetization increases from $\sim 1.25\mu_{Bohr}$/atom

to $\sim 2\mu_{\mathrm{Bohr}}/\mathrm{atom}$. Along with deposition step $i = 9$, the growth rate changes from $1.35\ \mathrm{nm}/(\mu\mathrm{g\,cm^{-2}})$ to $1.40\ \mathrm{nm}/(\mu\mathrm{g\,cm^{-2}})$. In their combination, these changes strongly indicate a magnetically driven phase transition from the face-centered-cubic (fcc) to the body-centered-cubic (bcc) phase that the Fe film undergoes at around $i = 9$. This phase transition is known to exist for Fe films with a thickness of ~10–12 atomic layers [41,46,54].

Growing further, all properties of the film stay remarkably constant. Its magnetization equals $\sim 2\mu_{\mathrm{Bohr}}/\mathrm{atom}$, which is close to the bulk value of $\sim 2.2\mu_{\mathrm{Bohr}}/\mathrm{atom}$ of Fe.

IV. SUMMARY AND CONCLUSIONS

We probe the magnetic and structural properties of a thin film of Fe that is epitaxially grown in UHV on a $\mathrm{Cu}(001)_{45\ \mathrm{nm}}/\mathrm{Si}(001)$ substrate using *in situ* PNR. The combination of Montel optics with dc magnetron sputtering in UHV allows the *in situ* collection of spin-polarized neutron data during the sequence of 22 growth steps while keeping the sample fixed in the neutron beam. Avoiding any movements of the sample is ideal for detecting small variations in the *in situ* PNR signal. Moreover, the analysis of the data is facilitated because it is based on one and the same sample.

Our *in situ* PNR measurements confirm most of the known thickness-dependent magnetic properties of Fe layers. However, we observe some unique features in our sputter-deposited Fe layers when compared with layers grown by other techniques. These include an indication for a large magnetization during the early nucleation phase that exceeds the literature values [50,51] by more than 10%. We also observe magnetism at room temperature in films with a thickness of 5 to 11 atomic layers, which corresponds to an increase of T_C of at least 20 K if compared to the T_C of the Fe films reported in the literature [46].

While the understanding of the evolution of Fe films during their growth is of interest in itself, our studies simultaneously demonstrate the viability and potential of *in situ* PNR for the analysis of magnetic properties on an atomic scale. Here, *in situ* PNR can clearly provide relevant data that complement the data obtained from photon and electron-based techniques. In fact, the future prospects of *in situ* PNR are tantalizing: possible scientific questions for *in situ* PNR include the investigation of perpendicular magnetic anisotropy [2], magnetoelastic coupling [3,4,55], and magnetism at oxide interfaces and the corresponding topology [5–7]. We expect that *in situ* PNR will also be of great benefit in the investigation of the buildup of chirality or incommensurability [56,57] or the formation of solitons and skyrmions in films or at interfaces [10,11] during growth.

In addition, the detailed observation of the processes taking place during topotactic transformations [1] or the formation of self-organized structures [58] can be followed up *in situ*. In this context, beam lines might, however, be preferable that in addition to reflectometry also allow large-angle scattering geometries. There, additionally to the data obtained by *in situ* PNR, crystal structures, including defects like oxygen vacancies, can be analyzed.

While we demonstrate the *in situ* technique using sputtering as the deposition method, *in situ* PNR is equally well applicable for MBE or pulsed laser deposition, in particular because the deposition of adatoms on chamber walls can more easily be minimized, thereby avoiding neutron activation. Compared with the setup presented in this work, an implementation of *in situ* PNR at the future European Spallation Source (ESS) using the next-generation Selene optics (to be realized for the reflectometer ESTIA [59] at ESS) will increase the flux at the sample by approximately a factor of 4000, thus decreasing the measuring time to below half a second for the two spin channels [60]. Therefore, *in situ* PNR will even provide sufficient time resolution for probing the structural and magnetic properties during thin-film growth, both *in situ* and *in operando*, thus opening fascinating applications in the field of thin films.

ACKNOWLEDGMENTS

This work is based on experiments performed on AMOR at the Swiss spallation source SINQ, Paul Scherrer Institut, Switzerland and upon experiments performed at the REFSANS instrument operated by HZG at the Heinz Maier-Leibnitz Zentrum (MLZ), Garching, Germany. Part of the work is supported by the Swiss National Science Foundation through the National Centre of Competence in Research MaNEP and by the Deutsche Forschungsgemeinschaft via the Transregional Research Center TRR80.

[1] Th. Mairoser, J. A. Mundy, A. Melville, D. Hodash, P. Cueva, R. Held, A. Glavic, J. Schubert, D. A. Muller, D. G. Schlom, and A. Schmehl, High-quality EuO thin films the easy way via topotactic transformation, Nat. Commun. **6**, 7716 (2015).

[2] S. Ikeda, K. Miura, H. Yamamoto, K. Mizunuma, H. D. Gan, M. Endo, S. Kanai, J. Hayakawa, F. Matsukura, and H. Ohno, A perpendicular-anisotropy CoFeB-MgO magnetic tunnel junction, Nat. Mater. **9**, 721 (2010).

[3] R. O. Cherifi, V. Ivanovskaya, L. C. Phillips, A. Zobelli, I. C. Infante, E. Jacquet, V. Garcia, S. Fusil, P. R. Briddon, N. Guiblin, A. Mougin, A. A. Ünal, F. Kronast, S. Valencia, B. Dkhil, A. Barthelemy, and M. Bibes, Electric-field control of magnetic order above room temperature, Nat. Mater. **13**, 345 (2014).

[4] X. R. Wang, C. J. Li, W. M. Lü, T. R. Paudel, D. P. Leusink, M. Hoek, N. Poccia, A. Vailionis, T. Venkatesan, J. M. D. Coey, E. Y. Tsymbal, Ariando, and H. Hilgenkamp, Imaging and control of ferromagnetism in $LaMnO_3/SrTiO_3$ heterostructures, Sci. Adv. **349**, 716 (2015).

[5] S. Thiel, G. Hammerl, A. Schmehl, C. W. Schneider, and J. Mannhart, Tunable quasi-two-dimensional electron gases in oxide heterostructures, Science **313**, 1942 (2006).

[6] N. Reyren, S. Thiel, A. D. Caviglia, K. L. Fitting, G. Hammerl, C. Richter, C. W. Schneider, T. Kopp, A.-S. Rüetschi, D. Jaccard, M. Gabay, D. A. Muller, J.-M. Triscone, and J. Mannhart, Superconducting interfaces between insulating oxides, Science **317**, 1196 (2007).

[7] A. Brinkman, M. Huijben, M. van Zalk, J. Huijben, U. Zeitler, J. C. Maan, W. G. van der Wiel, G. Rijnders, D. H. A. Blank, and H. Hilgenkamp, Magnetic effects at the interface between non-magnetic oxides, Nat. Mater. **6**, 493 (2007).

[8] J. F. Gregg, Spintronics: A growing science, Nat. Mater. **6**, 798 (2007).

[9] A. Schmehl, V. Vaithyanathan, A. Herrnberger, St. Thiel, Ch. Richter, M. Liberati, T. Heeg, M. Rckerath, L.-F. Kourkoutis, S. Mühlbauer, P. Bni, D. A. Muller, Y. Barash, J. Schubert, Y. Idzerda, J. Mannhart, and D. G. Schlom, Epitaxial integration of the highly spin-polarized ferromagnetic semiconductor EuO with silicon and GaN, Nat. Mater. **6**, 882 (2007).

[10] S. A. Meynell, M. N. Wilson, H. Fritzsche, A. N. Bogdanov, and T. L. Monchesky, Surface twist instabilities and skyrmion states in chiral ferromagnets, Phys. Rev. B **90**, 014406 (2014).

[11] E. A. Karhu, S. Kahwaji, M. D. Robertson, H. Fritzsche, B. J. Kirby, C. F. Majkrzak, and T. L. Monchesky, Helical magnetic order in MnSi thin films, Phys. Rev. B **84**, 060404 (2011).

[12] Y. F. Nie, Y. Zhu, C.-H. Lee, L. F. Kourkoutis, J. A. Mundy, J. Junquera, Ph. Ghosez, D. J. Baek, S. Sung, X. X. Xi, K. M. Shen, D. A. Muller, and D. G. Schlom, Atomically precise interfaces from non-stoichiometric deposition, Nat. Commun. **5**, 4530 (2014).

[13] S. Middey, J. Chakhalian, P. Mahadevan, J. W. Freeland, A. J. Millis, and D. D. Sarma, Physics of ultrathin films and heterostructures of rare-earth nickelates, Annu. Rev. Mater. Res. **46**, 305 (2016).

[14] M. Gibert, M. Viret, A. Torres-Pardo, C. Piamonteze, P. Zubko, N. Jaouen, J.-M. Tonnerre, A. Mougin, J. Fowlie, S. Catalano, A. Gloter, O. Stephan, and J.-M. Triscone, Interfacial control of magnetic properties at $LaMnO_3/LaNiO_3$ interfaces, Nano Lett. **15**, 7355 (2015).

[15] M. Mamoru Yoshimoto, H. Nagata, T. Tsukahara, and H. Koinuma, *In situ* RHEED observation of CeO_2 film growth on Si by laser ablation deposition in ultrahigh-vacuum, Jpn. J. Appl. Phys. **29**, L1199 (1990).

[16] W. Matz, N. Schell, W. Neumann, J. Bttiger, and J. Chevallier, A two magnetron sputter deposition chamber for *in situ* observation of thin film growth by synchrotron radiation scattering, Rev. Sci. Instrum. **72**, 3344 (2001).

[17] O. M. Magnussen, J. Hotlos, R. J. Nichols, D. M. Kolb, and R. J. Behm, Atomic Structure of Cu Adlayers on Au(100) and Au(111) Electrodes Observed by *In situ* Scanning Tunneling Microscopy, Phys. Rev. Lett. **64**, 2929 (1990).

[18] Ph. Lavalle, C. Gergely, F. J. G. Cuisinier, G. Decher, P. Schaaf, J. C. Voegel, and C. Picart, Comparison of the structure of polyelectrolyte multilayer films exhibiting a linear and an exponential growth regime: An in situ atomic force microscopy study, Macromolecules **35**, 4458 (2002).

[19] A. Syed Mohd, S. Pütter, S. Mattauch, A. Koutsioubas, H. Schneider, A. Weber, and T. Brückel, A versatile UHV transport and measurement chamber for neutron reflectometry under UHV conditions, Rev. Sci. Instrum. **87**, 123909 (2016).

[20] T. Nawrath, H. Fritzsche, F. Klose, J. Nowikow, and H. Maletta, In situ magnetometry with polarized neutrons on thin magnetic films, Phys. Rev. B **60**, 9525 (1999).

[21] J. A. Dura and J. LaRock, A molecular beam epitaxy facility for in situ neutron scattering, Rev. Sci. Instrum. **80**, 073906 (2009).

[22] B. R. Cuenya, W. Keune, D. Li, and S. D. Bader, Enhanced hyperfine magnetic fields for face-centered tetragonal Fe (110) ultrathin films on vicinal Pd(110), Phys. Rev. B **71**, 064409 (2005).

[23] A. Hahlin, C. Andersson, J. H. Dunn, B. Sanyal, O. Karis, and D. Arvanitis, Structure and magnetism of ultrathin epitaxial Fe on Ag(100), Phys. Rev. B **73**, 134423 (2006).

[24] C. C. Kuo, W. Pan, Y. C. Chen, and M.-T. Lin, Exchange bias in $Co/Fe/Fe_xMn_{1-x}/Cu(100)$ ultrathin films, J. Appl. Phys. **93**, 8743 (2003).

[25] M. Croft, D. Sills, A. Sahiner, A. F. Jankowski, P. H. Ansari, E. Kemly, F. Lu, Y. Jeon, and T. Tsakalakos, Fe-fcc layer stabilization in [111]-textured Fe/Pt multilayers, Nanostruct. Mater. **9**, 413 (1997).

[26] B. An, L. Zhang, S. Fukuyama, and K. Yokogawa, Growth and structural transition of Fe ultrathin films on Ni(111) investigated by LEED and STM, Phys. Rev. B **79**, 085406 (2009).

[27] T. Allmers and M. Donath, Magnetic properties of Fe films on flat and vicinal Au(111): Consequences of different growth behavior, Phys. Rev. B **81**, 064405 (2010).

[28] C. A. F. Vaz, J. A. C. Bland, and G. Lauhoff, Magnetism in ultrathin film structures, Rep. Prog. Phys. **71**, 056501 (2008).

[29] B. M. Clemens, T. C. Hufnagel, M. C. Kautzky, and J.-F. Bobo, in *Symposium CC—Thin Films Stresses and Mechanical Properties VI*, MRS Symposia Proceedings No. 436 (Materials Research Society, Warrendale, PA, 1996), pp. 9–20.

[30] J. Stahn, U. Filges, and T. Panzner, Focusing specular neutron reflectometry for small samples, Eur. Phys. J. Appl. Phys. **58**, 11001 (2012).

[31] J. Stahn and A. Glavic, Focusing neutron reflectometry: Implementation and experience on the TOF-reflectometer Amor, Nucl. Instrum. Methods Phys. Res., Sect. A **821**, 44 (2016).

[32] H. Jiang, T. J. Klemmer, J. A. Barnard, and E. A. Payzant, Epitaxial growth of Cu on Si by magnetron sputtering, J. Vac. Sci. Technol. A **16**, 3376 (1998).

[33] G. Gubbiotti, G. Carlotti, C. Minarini, S. Loreti, R. Gunnella, and M. De Crescenzi, Metal-metal epitaxy on silicon: Cu/Ni/Cu ultrathin films on 7×7-Si(111), Surf. Sci. **449**, 218 (2000).

[34] Chin-An Chang, Magnetocrystalline anisotropy of (100) face-centered cubic Co structures deposited on Cu/Si(100), Appl. Phys. Lett. **58**, 1745 (1991).

[35] P. Castrucci, R. Gunnella, R. Bernardini, A. Montecchiari, R. Carboni, and M. De Crescenzi, Epitaxy of Fe/Cu/Si(1 1 1) ultrathin films: An Auger electron diffraction study, Surf. Sci. **482–485**, 916 (2001).
[36] Chin-An Chang, Deposition of (100) Au, Ag, Pd, Pt, and Fe on (100) Si using different metal seed layers, J. Vac. Sci. Technol. A **9**, 98 (1991).
[37] Chin-An Chang, Interface epitaxy and self-epitaxy of metals near room temperatures, Phys. Rev. B **42**, 11946 (1990).
[38] Purity: 99.99999% (7N).
[39] Simulreflec—reflectivity curve simulations and fitting, http://www-llb.cea.fr/prism/programs/simulreflec/simulreflec.html, accessed 2016-02-25.
[40] Matts Björck and Gabriella Andersson, GenX: An extensible x-ray reflectivity refinement program utilizing differential evolution, J. Appl. Crystallogr. **40**, 1174 (2007).
[41] J. Giergiel, J. Kirschner, J. Landgraf, J. Shen, and J. Woltersdorf, Stages of structural transformation in iron thin film growth on copper (100), Surf. Sci. **310**, 1 (1994).
[42] A. Enders, D. Peterka, D. Repetto, N. Lin, A. Dmitriev, and K. Kern, Temperature Dependence of the Surface Anisotropy of Fe Ultrathin Films on Cu(001), Phys. Rev. Lett. **90**, 217203 (2003).
[43] D. Li, M. Freitag, J. Pearson, Z. Q. Qiu, and S. D. Bader, Magnetic Phases of Ultrathin Fe Grown on Cu(100) as Epitaxial Wedges, Phys. Rev. Lett. **72**, 3112 (1994).
[44] D. Qian, X. F. Jin, J. Barthel, M. Klaua, and J. Kirschner, Spin-Density Wave in Ultrathin Fe Films on Cu(100), Phys. Rev. Lett. **87**, 227204 (2001).
[45] S. Müller, P. Bayer, C. Reischl, K. Heinz, B. Feldmann, H. Zillgen, and M. Wuttig, Structural Instability of Ferromagnetic fcc Fe Films on Cu(100), Phys. Rev. Lett. **74**, 765 (1995).
[46] J. Thomassen, F. May, B. Feldmann, M. Wuttig, and H. Ibach, Magnetic Live Surface Layers in Fe/Cu(100), Phys. Rev. Lett. **69**, 3831 (1992).
[47] S. Bhagwat, R. Thamankar, and F. O. Schumann, Evidence for superparamagnetism in ultrathin Fe and Fe_xMn_{1-x} films on Cu (1 0 0), J. Magn. Magn. Mater. **290–291**, 216 (2005).
[48] J. Shen, R. Skomski, M. Klaua, H. Jenniches, S. Sundar Manoharan, and J. Kirschner, Magnetism and morphology of Fe/Cu(111) films below two-dimensional percolation, J. Appl. Phys. **81**, 3901 (1997).
[49] K. Heinz, S. Müller, and P. Bayer, Iron multilayers on Cu(100)—A case of complex reconstruction investigated by quantitative LEED, Surf. Sci. **352–354**, 942 (1996).
[50] Chun Li, A. J. Freeman, H. J. F. Jansen, and C. L. Fu, Magnetic anisotropy in low-dimensional ferromagnetic systems: Fe monolayers on Ag(001), Au(001), and Pd (001) substrates, Phys. Rev. B **42**, 5433 (1990).
[51] Chun Li and A. J. Freeman, Giant monolayer magnetization of Fe on MgO: A nearly ideal two-dimensional magnetic system, Phys. Rev. B **43**, 780 (1991).
[52] M. Wuttig and X. Liu, *Ultrathin Metal Films* (Springer, Berlin, Heidelberg, 2004), Vol. 206.
[53] S. V. Komogortsev, S. N. Varnakov, S. A. Satsuk, I. A. Yakovlev, and S. G. Ovchinnikov, Magnetic anisotropy in Fe films deposited on SiO2/Si(001) and Si(001) substrates, J. Magn. Magn. Mater. **351**, 104 (2014).
[54] Th. Detzel, N. Memmel, and Th. Fauster, Growth of ultrathin iron films on Cu(001): An ion-scattering spectroscopy study, Surf. Sci. **293**, 227 (1993).
[55] M.-B. Lepetit, B. Mercey, and C. Simon, Interface Effects in Perovskite Thin Films, Phys. Rev. Lett. **108**, 087202 (2012).
[56] S. V. Maleyev, Investigation of Spin Chirality by Polarized Neutrons, Phys. Rev. Lett. **75**, 4682 (1995).
[57] S. V. Grigoriev, D. Lott, Yu. O. Chetverikov, A. T. D. Grünwald, R. C. C. Ward, and A. Schreyer, Interplay of RKKY, Zeeman, and Dzyaloshinskii-Moriya interactions and the nonzero average spin chirality in Dy/Y multilayer structures, Phys. Rev. B **82**, 195432 (2010).
[58] J. C. Denardin, E. Burgos, R. Lavin, S. Vojkovic, J. Briones, and M. Flores, Magnetic properties of Co/Cu/Py antidot films with different pore diameters, IEEE Trans. Magn. **50**, 1 (2014).
[59] J Stahn and M. Cárdenas, "Estia—focusing reflectometer," ESS Instrument Construction Proposal, European Spallation Source ESS AB, Lund, Sweden, 2013.
[60] The gain of 4000 at ESS when compared with SINQ is obtained as follows: 100 times larger peak brilliance, 10 times larger beam area (20 mm × 20 mm), and a 4 times larger solid angle. Moreover, a larger range of momentum transfers q_z is probed.